Check for updates

BRIEF COMMUNICATION OPEN

Strain control of layer-resolved negative capacitance in superlattices

Raymond Walter [1,2,3 ✉], Sergey Prosandeev[1,4], Charles Paillard [1,5 ✉] and L. Bellaiche[1]

Negative capacitance in BaTiO$_3$/SrTiO$_3$ superlattices is investigated by Monte Carlo simulations in an atomistic effective Hamiltonian model, using fluctuation formulas for responses to the local macroscopic field that incorporates depolarizing fields. We show that epitaxial strain can tune the negative capacitance of the BaTiO$_3$ ferroelectric layer and the overall capacitance of the system. In addition, we predict and explain an original switching of the negative capacitance from the BaTiO$_3$ layer to the SrTiO$_3$ layer at low temperatures for intermediate strains.

INTRODUCTION

Negative capacitance (NC) has been a puzzling concept since 1976[1]. Its realization would revolutionize the design of energy-efficient transistors[2]. Up to now, the same strategy has been employed to realize NC in ferroelectric materials: one needs to control the charge, rather than the electric field, at the edge of the ferroelectric materials in order to explore otherwise unreachable region of the hysteresis loop[3]. This was achieved either (i) by introducing a load-resistance in the external circuit during switching to control the flow of charges[4–7], in what we should call transient NC, or (ii) by introducing a stiff dielectric layer stacked in series with a ferroelectric layer[8]. The latter architecture allows NC to be achieved even at low frequencies, and it is thus called quasi-static NC[3]. In a Landau description, NC arises in both cases from the ability to explore regions of negative curvature of the thermodynamic potential[9]. The concept was further analyzed in the early 2000s[10,11].

In this communication, we focus on the quasi-static NC in a (BaTiO$_3$)$_m$/(SrTiO$_3$)$_n$ (BT/ST) superlattice (SL) architecture, and we demonstrate that, in addition to temperature (as shown in PbTiO$_3$/SrTiO$_3$ SLs in ref. [8]), strain allows as well to control the emergence of NC. BT/ST SLs are particularly interesting as they do not involve toxic element, such as lead, and possess a rich phase diagram[12,13].

RESULTS

Phase diagram

In order to achieve an atomistic understanding of the NC effect in SLs, we use Monte Carlo simulations based on an effective Hamiltonian to describe a BT$_8$/ST$_2$ SL (see "Methods" section). The phase diagram of such SL is depicted in Fig. 1. It shows: (1) a high-temperature paraelectric phase p; (2) an orthorhombic state with in-plane polarization (aa) for large tensile strains and low temperature; (3) alternating out-of-plane polar domains in addition to an in-plane polarization (ii) for large tensile to small compressive strains and low temperature; (4) out-of-plane polar domains with no in-plane polarization for moderate and larger compressive strain (i phase); and (5) at large compressive strain, a

monodomain phase with (green shaded area) or without (i') polar nanobubbles. The phase diagram agrees qualitatively with previous reports[12,13], except that a monodomain and polar nanobubbles are found, likely because our studied system has smaller overall Sr concentration than in those studies.

Local dielectric constant

We now turn our attention to the dielectric response of the different layers of our SL at 50 K for different strains. The local/internal dielectric constants, defined in the "Methods" section, are computed from linear response theory.

We plot the inverse of the internal dielectric response $1/\varepsilon_{33}^{int}$ (see "Methods" section for the precise definition of different physical quantities) as a function of strain, and at 50 K, in Fig. 2. The inverse dielectric response therein is decomposed into the BT layer (red circles), the ST layer (blue squares), and the BT/ST interface layer (orange diamonds) responses. The total (external) inverse dielectric response of the SL is shown in black circles. We can observe that, at tensile strain >1.2%, the BT layer exhibits negative dielectric constant, hence NC. Interestingly, when further reducing the tensile strain, and down to compressive strain of $\approx-0.9\%$, the ST layer now exhibits NC.

Looking at the total response of SL, in black circles in Fig. 2, we observe that the dielectric constant (and hence the total capacitance) is greatly enhanced in the region where the BT layer exhibits NC, which is exactly the intended effect, useful in the so-called NC field-effect transistor proposed by Salahuddin and Datta[2]. On the other hand, despite the negative dielectric response of the ST layer, the total dielectric constant decreases owing to the large decrease in the BT layer's internal dielectric response and its larger thickness compared to the ST layer. The importance of the thick BT layer in determining the global response of the SL is also responsible for the response of the interfacial layer that follows the response of the ST layer, as explained in Supplementary Note 3. It remains, however, extremely interesting to observe that careful engineering of SLs combining "weak" (such as STO) and "hard" (such as BTO)

[1]Department of Physics and Institute for Nanoscience and Engineering, University of Arkansas, Fayetteville, AR 72701, USA. [2]Department of Mathematical Sciences, University of Arkansas, Fayetteville, AR 72701, USA. [3]Identity Engineering, Kinesso LLC, Conway, AR 72032, USA. [4]Institute of Physics and Physics Department of Southern Federal University, Rostov-na-Donu 344090, Russia. [5]Laboratoire Structures, Propriétés et Modélisation des Solides, CentraleSupélec, UMR CNRS 8580, Université Paris-Saclay, 91190 Gif-sur-Yvette, France. ✉email: rwalter@uark.edu; charles.paillard@centralesupelec.fr
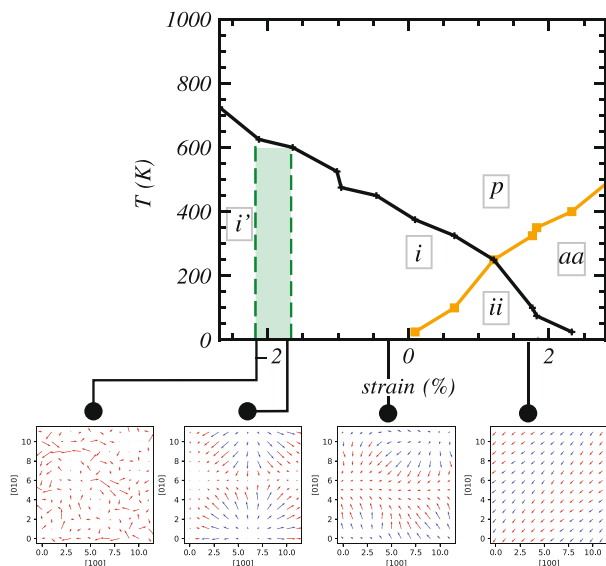
Fig. 1 Phase diagram of SL. Phase diagram of SL, with multidomain out-of-plane polar phase *i*, monodomain out-of-plane polar phase *i'*, orthorhombic polar phase with in-plane polarization *aa*, phase *ii* having both in-plane polarization and out-of-plane polar domains, and high-temperature paraelectric phase *p*. The black and yellow lines separate these phases. The green shaded area demarcates the stability region of polar nanobubbles. In-plane dipolar patterns are depicted for −2.02, −1.56, −0.45 and 1.77% epitaxial strains at 5 K and shows up (red) and down (blue) dipoles. Both in-plane and out-of-plane dipole patterns can be found in Supplementary Fig. 1.
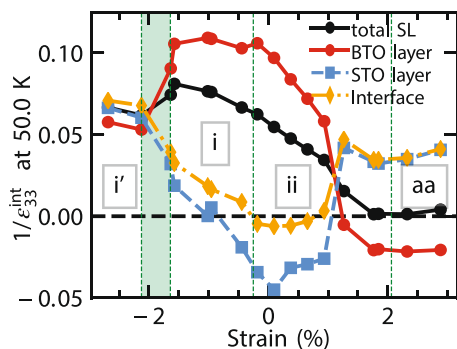

Fig. 2 Inverse local dielectric constant. Inverse local dielectric constant $1/\varepsilon_{layer}^{int}$ of the BT (red circles), ST (blue squares), and interfacial (orange diamonds) layers for different strains at 50 K in the BT/ST SL (black circles).

ferroelectric may be an avenue to increase the range of existence of the NC regime.

DISCUSSION

When discussing the origin of the switching of the NC from the BT to the ST layer, it is important to keep in mind that, in our parametrization of the effective Hamiltonian, the strontium titanate layer would exhibit a ferroelectric behavior at zero strain. This is due to the absence of quantum fluctuations and oxygen octahedra tilting degrees of freedom, known to work against the appearance of a low-temperature ferroelectric phase in SrTiO$_3$[14,15]. Several mechanisms contributing to NC in dielectric/ferroelectric layers were proposed[3,16]. At first, when cooling from the high-temperature paraelectric state to below the bulk transition temperature, the ferroelectric layer is frustrated into a null
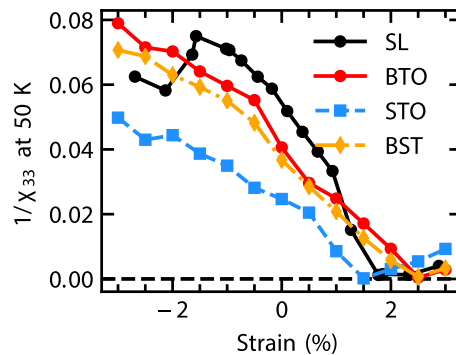

Fig. 3 Inverse out-of-plane dielectric susceptibility. Inverse out-of-plane dielectric susceptibility χ_{33}^{-1} for bulk STO (blue squares), bulk BTO (red circles), bulk BST (orange diamonds), and the SL (black circles). The strain is calculated with respect to the same equilibrium lattice constant defined in the "Methods" section.

polarization state if the dielectric is stiff enough. The ferroelectric is then said to be in an incipient state[3,8]. Upon further cooling, the ferroelectric adopts a multidomain configuration under a certain temperature $T_{\uparrow\downarrow}$. The poly-domain state below this transition has the soft structure with a gradual distribution of polarization as it has been proposed in refs. [17,18] and is visually seen from Fig. 1. Additional cooling may or may not result in the disappearance of the NC state, which so far is not well understood.

In our case, we observe similar behaviors, except they are strain-driven rather than temperature-driven. Indeed, at large tensile strain, the ST layer is paraelectric in the out-of-plane direction and thus acts as a stiff dielectric layer. On the other hand, a pure BT layer at lattice constants corresponding to a tensile strain between 1 and 3% would be ferroelectric but is here frustrated either in a multidomain state *ii* or in an incipient ferroelectric state *aa* (with respect to the out-of-plane direction) by the ST layer in the SL architecture. This results in the NC of the BT layer only.

Upon relaxing the tensile strain or entering the compressive strain regime (up to −1%), the BT layer remains in its multidomain state. However, the BT layer now exhibits positive capacitance, while the ST layer exhibits NC. According to Eq. (6), the only explanation for the NC switching from the BT to the ST layer is that the ST layer out-of-plane polar response is much stronger than the overall response of the heterostructure. Such criterion had already been worked out in previous works such as ref. [8] and is recalled in Eq. (6) in the "Methods" section. The existence of such a dramatic increase in the ST layer external susceptibility is the existence of a polar phase transition in STO upon biaxial compression, with dipole moments pointing out-of-plane. Indeed, strained bulk STO already exhibits a phase transition around 1.5% tensile strain within our numerical model and given our chosen reference lattice constant (see Fig. 3). In Fig. 3, we plot the response of bulk STO (blue square) compared to that of bulk BTO (red circles), BST solid solution (orange diamonds), and our BST SL (black square). It becomes apparent that the dielectric susceptibility of bulk STO becomes much larger than that of BT and the SL. Although different electrical boundary conditions shift the transition toward more compressive strain, the transition in bulk STO also occurs in the ST layer of the BST SL. The large dielectric response of the ST layer close to the transition (larger than the total dielectric constant of the SL) is likely the cause of the switch of the NC from the BT to the ST layer under more compressive strains. Note that long- and short-range interfacial effects in the BST SL broaden the ferroelectric transition in each material comprising the system. Indeed, although strained bulk BT exhibits an out-of-plane ferroelectric transition around 2.5% tensile strain, NC of the BT layer in Fig. 2 extends beyond that point. We must stress that it is the relative response of the layer compared to the response of the

whole system that determines the appearance of NC (see "Methods" section). Even beyond the transition of strained bulk BT, if long- and short-range interfacial effects sufficiently enhance the external dielectric response in the BT layer, it may happen that the fluctuations are large enough close to the transition to induce an NC state in the layer.

Note that the role of the BT layer in frustrating the polar transition of the ST layer is essential to achieve the NC switching. Indeed, as shown in the Supplementary Fig. 2, smaller BT/ST layer thickness ratio in the SL lead to a smaller and less extended NC in the ST layer. This also reveals that one must be extremely careful when using ST as a dielectric layer to measure the NC effect in a ferroelectric, as in ref. [8]. Indeed, it is apparent in our particular case that, at a specific strain, the dielectric constant of the ST layer can vary quite a lot depending on the ferroelectric layer/dielectric layer thickness ratio.

In summary, our first-principles-based effective Hamiltonian calculations reveal the existence of negative internal dielectric permittivities in the BT layer of a BT/ST SL. These quantities are associated with quasi-static negative differential capacitance and allow the tuning of overall capacitance. We further predict a previously unreported switching that exchanges the NC between the BT and ST layers at moderate biaxial strains (between −1 and +1%), associated with the onset of ferroelectricity in the ST layer under more compressive/less tensile strains than the BT layer. Our predictions can be checked experimentally by growing BT/ST SLs on top of various substrates such as $SrTiO_3$, $DyScO_3$, $GdScO_3$, $KTaO_3$, or $NdScO_3$ to explore biaxial strains ranging from −2 to +1%.

METHODS

Effective Hamiltonian and numerical parameters
We use the effective Hamiltonian model of ref. [19] that expresses the total energy as $H_{eff} = H_{ave}(\{u_i\}, \{v_i\}, \eta_H) + H_{loc}(\{u_i\}, \{v_i\}, \{\sigma_i\})$ in terms of a few degrees of freedom: the local soft mode in a unit cell i, u_i, proportional to the polarization; inhomogeneous strain describing the deformation of unit cell i, v_i; and the homogeneous strain η_H of the supercell. H_{ave} represents the average total energy of a $\langle Ba_{0.5}Sr_{0.5}\rangle TiO_3$ crystal in the virtual crystal approximation[20].

This model accurately described Curie temperatures and phase diagrams in disordered and ordered (Ba, Sr)TiO_3 systems[12,13,19], with the proviso that it predicts for $SrTiO_3$ an unstrained bulk paraelectric-to-ferroelectric transition around 100 K because it ignores quantum effects and octahedral rotations. This effective Hamiltonian model is, essentially, not very different than the method employed by Zubko et al.[8] to successfully simulate and experimentally verify the existence of quasi-static NC in their $PbTiO_3$/$SrTiO_3$ SL. Thus similar models have already proved good enough to capture the essential physics of NC in such systems.

We solve this effective Hamiltonian model using Metropolis Monte Carlo (MC) simulations in a $12 \times 12 \times 10$ supercell to mimic a $(BaTiO_3)_8$/$(SrTiO_3)_2$ SL grown along the pseudo-cubic [001] direction. The supercell is field cooled in the out-of-plane direction with a magnitude of the electric field of 200 kV cm^{-1}, from 1000 to 25 K by 25 K steps using 2×10^5 MC sweeps, and then to 5 K in 5 K steps using 10^6 sweeps. The field is then removed, and the system is heated from 5 to 25 K (5 K steps), and from 25 to 50 K (25 K steps) using 10^6 sweeps. Thermodynamic averages are taken over the last 8×10^5 sweeps.

In particular, we focus on the response of the system to an applied electric field at 50 K. Here biaxial strain of the SL is enforced by keeping the in-plane lattice constant of the SL fixed for any temperature and defined with respect to an absolute reference. This absolute reference is the lattice constant of cubic (Ba$_{0.8}$Sr$_{0.2}$)TiO_3 bulk at 0 K. As a result, this is not the misfit strain often considered in experiments, which is defined as the relative change of lattice constant between the extrapolated free SL lattice constant and the substrate. The real misfit strain is thus subject to the thermal evolution of the substrate lattice constant and is often not constant throughout a large temperature range.

Dielectric response estimation
Static dielectric susceptibilities are estimated based on linear response theory. Hence, we focus on the small signal response of the polarization to an applied field. In other words, we investigate quasi-static differential NC.

We focus on the dielectric response of the SL in different regions of the phase diagram at 50 K. Unlike the global dielectric permittivity of a solid modeled with periodic boundary conditions (i.e., neglecting surface effects), the layers of that system each experience a local depolarizing field in response to an applied electric field. Then the macroscopic electric field in the layer (which is not the microscopic dipole field in our effective Hamiltonian[21]) divides into a local part E_{loc} and an externally applied field E_{ext}. The overall macroscopic field in a specific layer (e.g., the BT or ST layers) can thus be written as $E_{layer} = E_{loc} + E_{ext}$. One can thus define external and internal susceptibilities for a layer, $\chi_{layer}^{ext} = \frac{\Delta P_{layer}}{\varepsilon_0 \Delta E_{ext}}$ and $\chi_{layer}^{int} = \frac{\Delta P_{layer}}{\varepsilon_0 \Delta E_{layer}}$, where ΔE_{layer} and ΔP_{layer} are the changes of total electric field and polarization in the layer in reaction to an applied external electric field ΔE_{ext}, respectively[22,23]. All electric fields and polarizations are considered along the pseudo-cubic [001] direction. The (potentially layer-decomposed) susceptibilities and dielectric constants are responses to macroscopic electric fields, similarly to the approach of ref. [8]. As such, we use the following linear response formulas (see Supplementary Material) to calculate those responses:

$$\chi_{layer}^{ext} = \frac{1}{\varepsilon_0} \frac{V}{k_B T} \left[\langle P_{layer} P_{tot} \rangle - \langle P_{layer} \rangle \langle P_{tot} \rangle \right], \tag{1}$$

$$\chi_{layer}^{int} = \chi_{layer}^{ext} / \frac{\partial \langle E_{layer} \rangle}{\partial E_{ext}}. \tag{2}$$

The total volume factor is V; T and k_B refer to temperature and Boltzmann's constant, respectively; angular brackets indicate thermodynamic averages. One can define an internal dielectric permittivity $\varepsilon_{layer}^{int}$ for a layer in addition to the total dielectric permittivity ε_{tot} of the system,

$$\varepsilon_{layer}^{int} = 1 + \chi_{layer}^{int}, \tag{3}$$

$$\varepsilon_{tot} = 1 + \frac{1}{\varepsilon_0} \frac{V}{k_B T} \left[\langle P_{tot}^2 \rangle - \langle P_{tot} \rangle^2 \right]. \tag{4}$$

We rely upon a fluctuation formula (see Supplementary Material) for the response of the internal electric field to the external electric field:

$$\frac{\partial \langle E_{layer} \rangle}{\partial E_{ext}} = 1 + \frac{V}{k_B T} [\langle E_{loc} P_{tot} \rangle - \langle E_{loc} \rangle \langle P_{tot} \rangle] \tag{5}$$

$$= \varepsilon_{tot} - \chi_{layer}^{ext} \quad \text{(periodic SL)}. \tag{6}$$

Equation (5) applies under general electrical boundary conditions that are not necessarily periodic. In a periodic SL as considered here, $E_{loc} = (P_{tot} - P_{layer})/\varepsilon_0$[8]; then, upon substituting Eq. (6) into Eq. (2), we recover the formula for the internal relative dielectric permittivity $\varepsilon_{layer}^{int} = \varepsilon_{tot}/(\varepsilon_{tot} - \chi_{layer}^{ext})$ in ref. [8]. Equations (2), (3), and (5) imply one can achieve NC if $\frac{\partial \langle E_{layer} \rangle}{\partial E_{ext}} < 0$, when the change in residual depolarizing field in the layer ΔE_{loc} caused by an applied field E_{ext} is larger in magnitude than E_{ext}[22,23]. In the supplement, we compare direct and statistical approaches to calculating $\varepsilon_{layer}^{int}$ and derive a series capacitance sum rule that let us interpret NC in terms of a negative $\varepsilon_{layer}^{int}$.

REFERENCES

1. Landauer, R. Can capacitance be negative? *Collect. Phenom.* **2**, 167–170 (1976).
2. Salahuddin, S. & Datta, S. Use of negative capacitance to provide voltage amplification for low power nanoscale devices. *Nano Lett.* **8**, 405–410 (2008).
3. Íñiguez, J., Zubko, P., Luk'yanchuk, I. & Cano, A. Ferroelectric negative capacitance. *Nat. Rev. Mater.* **4**, 234–256 (2019).
4. Khan, A. I. et al. Negative capacitance in a ferroelectric capacitor. *Nat. Mater.* **14**, 182–186 (2015).
5. Hoffmann, M. et al. Direct observation of negative capacitance in polycrystalline ferroelectric HfO$_2$. *Adv. Func. Mater.* **26**, 8643–8649 (2016).
6. Hoffmann, M. et al. Ferroelectric negative capacitance domain dynamics. *J. Appl. Phys.* **123**, 184101 (2018).
7. Chang, S.-C., Avci, U. E., Nikonov, D. E., Manipatruni, S. & Young, I. A. Physical origin of transient negative capacitance in a ferroelectric capacitor. *Phys. Rev. Appl.* **9**, 014010 (2018).
8. Zubko, P. et al. Negative capacitance in multidomain ferroelectric superlattices. *Nature* **534**, 524–528 (2016).
9. Krowne, C. M., Kirchoefer, S. W., Chang, W., Pond, J. M. & Alldredge, L. M. B. Examination of the possibility of negative capacitance using ferroelectric materials in solid state electronic devices. *Nano Lett.* **11**, 988–992 (2011).
10. Bratkovsky, A. M. & Levanyuk, A. P. Very large dielectric response of thin ferroelectric films with the dead layers. *Phys. Rev. B* **63**, 132103 (2001).
11. Bratkovsky, A. M. & Levanyuk, A. P. Depolarizing field and "real" hysteresis loops in nanometer-scale ferroelectric films. *Appl. Phys. Lett.* **89**, 253108 (2006).
12. Lisenkov, S. & Bellaiche, L. Phase diagrams of BaTiO$_3$ SrTiO$_3$ superlattices from first principles. *Phys. Rev. B* **76**, 020102(R) (2007).
13. Choudhury, N., Walizer, L., Lisenkov, S. & Bellaiche, L. Geometric frustration in compositionally modulated ferroelectrics. *Nature* **470**, 513–517 (2011).
14. Müller, K. A. & Burkard, H. SrTiO$_3$: an intrinsic quantum paraelectric below 4 K. *Phys. Rev. B* **19**, 3593–3602 (1979).
15. Bellaiche, L. & Íñiguez, J. Universal collaborative couplings between oxygen-octahedral rotations and antiferroelectric distortions in perovskites. *Phys. Rev. B* **88**, 014104 (2013).
16. Cano, A. & Jiménez, D. Multidomain ferroelectricity as a limiting factor for voltage amplification in ferroelectric field-effect transistors. *Appl. Phys. Lett.* **97**, 133509 (2010).
17. De Guerville, F., Luk'yanchuk, I., Lahoche, L. & El Marssi, M. Modeling of ferroelectric domains in thin films and superlattices. *Mater. Sci. Eng. B* **120**, 16 (2005).
18. Luk'yanchuk, I. A., Lahoche, L. & Sené, A. Universal properties of ferroelectric domains. *Phys. Rev. Lett.* **102**, 147601 (2009).
19. Walizer, L., Lisenkov, S. & Bellaiche, L. Finite-temperature properties of (Ba,Sr)TiO$_3$ systems from atomistic simulations. *Phys. Rev. B* **73**, 144105 (2006).
20. Bellaiche, L. & Vanderbilt, D. Virtual crystal approximation revisited: Application to dielectric and piezoelectric properties of perovskites. *Phys. Rev. B* **61**, 7877–7882 (2000).
21. Ponomareva, I., Naumov, I. I., Kornev, I., Fu, H. & Bellaiche, L. Atomistic treatment of depolarizing energy and field in ferroelectric nanostructures. *Phys. Rev. B* **72**, 140102(R) (2005).
22. Ponomareva, I., Bellaiche, L. & Resta, R. Relation between dielectric responses and polarization fluctuations in ferroelectric nanostructures. *Phys. Rev. B* **76**, 235403 (2007).
23. Ponomareva, I., Bellaiche, L. & Resta, R. Dielectric anomalies in ferroelectric nanostructures. *Phys. Rev. Lett.* **99**, 227601 (2007).

AUTHOR CONTRIBUTIONS

L.B. proposed and designed the study. R.W. and S.P. performed the simulations. All authors discussed and analyzed the results and participated in writing the present manuscript.

COMPETING INTERESTS

The authors declare no competing interests.

ADDITIONAL INFORMATION

Supplementary information is available for this paper at https://doi.org/10.1038/s41524-020-00459-4.

Correspondence and requests for materials should be addressed to R.W. or C.P.

Reprints and permission information is available at http://www.nature.com/reprints

Publisher's note Springer Nature remains neutral with regard to jurisdictional claims in published maps and institutional affiliations.